Cellulose-Pectin Spatial Contacts Are Inherent to Never-Dried Arabidopsis Primary Cell Walls: Evidence from Solid-State Nuclear Magnetic Resonance[1][OPEN]

Tuo Wang, Yong Bum Park, Daniel J. Cosgrove*, and Mei Hong*

Department of Chemistry, Massachusetts Institute of Technology, Cambridge, Massachusetts 02139 (T.W., M.H.); and Department of Biology, Pennsylvania State University, University Park, Pennsylvania 16802 (Y.B.P., D.J.C.)

ORCID ID: 0000-0002-4020-5786 (D.J.C.).

The structural role of pectins in plant primary cell walls is not yet well understood because of the complex and disordered nature of the cell wall polymers. We recently introduced multidimensional solid-state nuclear magnetic resonance spectroscopy to characterize the spatial proximities of wall polysaccharides. The data showed extensive cross peaks between pectins and cellulose in the primary wall of Arabidopsis (*Arabidopsis thaliana*), indicating subnanometer contacts between the two polysaccharides. This result was unexpected because stable pectin-cellulose interactions are not predicted by in vitro binding assays and prevailing cell wall models. To investigate whether the spatial contacts that give rise to the cross peaks are artifacts of sample preparation, we now compare never-dried Arabidopsis primary walls with dehydrated and rehydrated samples. One-dimensional ^{13}C spectra, two-dimensional ^{13}C-^{13}C correlation spectra, water-polysaccharide correlation spectra, and dynamics data all indicate that the structure, mobility, and intermolecular contacts of the polysaccharides are indistinguishable between never-dried and rehydrated walls. Moreover, a partially depectinated cell wall in which 40% of homogalacturonan is extracted retains cellulose-pectin cross peaks, indicating that the cellulose-pectin contacts are not due to molecular crowding. The cross peaks are observed both at −20°C and at ambient temperature, thus ruling out freezing as a cause of spatial contacts. These results indicate that rhamnogalacturonan I and a portion of homogalacturonan have significant interactions with cellulose microfibrils in the native primary wall. This pectin-cellulose association may be formed during wall biosynthesis and may involve pectin entrapment in or between cellulose microfibrils, which cannot be mimicked by in vitro binding assays.

Despite decades of research, many aspects of the three-dimensional (3D) structure of the primary cell walls (CWs) of eudicotyledons and noncommelinid monocotyledons remain uncertain because of the insoluble, amorphous, and complex nature of CW polymers and their tight interactions in muro (Jarvis, 1992; Cosgrove, 2005). Unlike massively cross-linked bacterial CWs, noncovalent interactions between polysaccharides play major structural roles in plant CWs (Albersheim et al., 2011). Our concepts of the arrangement and interactions of cellulose, hemicellulose, and pectins in the CW have largely been shaped by electron microscopy and by chemical or enzymatic dissections, approaches that are limited in their ability to resolve specific noncovalent interactions or that result in considerable perturbation of native CW structures (McCann et al., 1990; Talbott and Ray, 1992; Carpita and Gibeaut, 1993). Recently, two-dimensional (2D) and 3D solid-state nuclear magnetic resonance (SSNMR) techniques have been applied to study the 3D architecture of plant CW polysaccharides (Dick-Pérez et al., 2011, 2012; Wang et al., 2014). The SSNMR experiments detect polysaccharide conformation, mobility, and subnanometer interatomic contacts, and the measurements were done on CW samples that were minimally perturbed from the native state. Interestingly, the 2D and 3D ^{13}C correlation spectra showed clear cross peaks between cellulose and Rha or galacturonic acid residues of pectic polysaccharides. Together with molecular dynamics simulations (Matthews et al., 2006; Zhao et al., 2014) and enzymatic and biomechanical analyses (Park and Cosgrove, 2012a, 2012b), these data led to a revised concept of the CW architecture in which cellulose makes physical contact with both xyloglucan and pectins and in which CW extensibility is controlled at limited biomechanical hotspots where multiple microfibrils come into close contact (Cosgrove,

[1] This work was supported by the Center for Lignocellulose Structure and Formation, an Energy Frontier Research Center funded by the U.S. Department of Energy, Office of Science, Basic Energy Sciences (grant no. DE–SC0001090). The 900-MHz spectra were measured at the Massachusetts Institute of Technology/Harvard Center for Magnetic Resonance, which is supported by the National Institutes of Health (grant no. EB002026).

* Address correspondence to dcosgrove@psu.edu and meihong@mit.edu.

The author responsible for distribution of materials integral to the findings presented in this article in accordance with the policy described in the Instructions for Authors (www.plantphysiol.org) is: Daniel J. Cosgrove (dcosgrove@psu.edu).

Y.B.P. produced the plant cell wall samples; T.W. performed the solid-state NMR experiments; all authors analyzed the data and wrote the article; D.J.C. and M.H. conceived the project.

[OPEN] Articles can be viewed without a subscription.

www.plantphysiol.org/cgi/doi/10.1104/pp.15.00665

2014). This new model contrasts with the prevailing tethered network model, which depicts a scaffold of cellulose microfibrils tethered by xyloglucans and embedded in a separate but coextensive gel-like phase made of pectin (Carpita and Gibeaut, 1993; Somerville et al., 2004; Cosgrove, 2005). Additional SSNMR data demonstrated that expansins target limited sites in the CW with altered cellulose conformation and enriched xyloglucan content (Wang et al., 2013), sites that are very similar to the hypothesized biomechanical hotspots (Park and Cosgrove, 2012b).

Despite these advances, the structural roles of pectins in the CW remain puzzling and unresolved. The major pectic polysaccharides include homogalacturonan (HG), rhamnogalacturonan I (RGI), and rhamnogalacturonan II (Caffall and Mohnen, 2009). Neutral pectins, including arabinans and galactans, are found as side chains of RGI and possibly as free polymers. Rhamnogalacturonan II units are cross linked by borate diesters that influence the strength and porosity of primary CWs (Ishii and Matsunaga, 1996; Fleischer et al., 1999). Some pectins may be covalently linked to arabinogalactan proteins (Tan et al., 2013) or xyloglucan (Popper and Fry, 2008; Cornuault et al., 2014), but the prevalence and structural significance of such hybrid molecules remain to be determined. Early extraction studies of a number of plant CWs showed that pectic polysaccharides remained with cellulose in the unextracted residue (Ryden and Selvendran, 1990; Goodneratne et al., 1994), and galactan side chains remain highly mobile in extracted onion (*Allium cepa*) CWs, which indirectly suggests that pectins may attach to cellulose via the rhamnogalacturonan backbone or HG (Foster et al., 1996). However, these results were not accounted for in traditional CW structural models (Cosgrove, 2001), which depict pectins as a relatively compliant gel-like network in which the cellulose-xyloglucan network is embedded. In this view, interactions between the two networks are limited to polymer entanglements and do not include extensive noncovalent interactions. Supporting this model are in vitro binding studies that indicate negligible affinity between pectins and cellulose, in contrast to the high affinity between xyloglucan and cellulose (Zykwinska et al., 2005, 2008). The recent 2D and 3D SSNMR spectra showed a significant number of cross peaks between cellulose and pectins (Dick-Perez et al., 2011, 2012), indicating that some of the pectic sugars come into subnanometer contact with cellulose. While NMR cross peaks report interatomic distances and not binding energies, the cross peaks nevertheless suggest that significant interactions exist between cellulose and some of the pectins. Such interactions, if true, would disagree with the in vitro binding assays but would be consistent with the early extraction results.

An unexpected result such as this one naturally meets with skepticism and a search for alternative explanations. One possibility is that the preparation of the first CW samples, which included washing with ethanol and other organic solvents followed by air drying and rehydration, might have caused pectins to precipitate irreversibly onto cellulose and other wall components, thus giving rise to artificial spatial contacts between different polymers. A second possibility is that the intermolecular contacts result from molecular crowding of the wall polymers rather than specific interactions stabilized by hydrogen bonding, van der Waals interactions, or other noncovalent interactions (Cosgrove, 2014). Binding assays indicate that neutral arabinan and galactan side chains of RGI moderately bind cellulose in vitro (Zykwinska et al., 2005, 2008), leading to the proposal that pectic side chains may function as structural linkers between cellulose microfibrils (Zykwinska et al., 2007; Peaucelle et al., 2012). Although the mechanical significance of pectins was not confirmed by experiments in which wild-type Arabidopsis (*Arabidopsis thaliana*) CWs were subjected to pectin-loosening treatments, pectins assumed a larger mechanical role in xyloglucan-deficient CWs (Park and Cosgrove, 2012a).

In this work, we investigate the nature of the pectin-cellulose contacts in greater depth by carrying out SSNMR experiments on a new set of CW samples that allows us to assess the effects of sample preparation, hydration history, temperature, and polysaccharide density on the cellulose-pectin spatial contacts. We prepared Arabidopsis primary CWs that were never dried throughout the sample preparation. We show that ^{13}C chemical shifts, intramolecular and intermolecular cross peaks, segmental order parameters, and nuclear spin relaxation times are indistinguishable between the never-dried and rehydrated walls. Difference 2D spectra (Wang et al., 2015) that suppress intramolecular cross peaks are obtained that better reveal the intermolecular cross peaks between cellulose and pectins. Variable-temperature experiments show that cross peaks persist at ambient temperature, thus ruling out artifactual interaction by freezing. Finally, a partially HG-extracted CW retains cellulose-pectin correlation peaks, indicating that molecular crowding is not the main cause of the intermolecular contacts. Taken together, these data indicate that cellulose-pectin spatial proximity is an intrinsic feature of the never-dried primary CW, and some of the pectins may be entrapped within or between cellulose microfibrils.

RESULTS

We first compared the never-dried sample CW#1 with a previous sample, CW#4, which was prepared from a different batch of plant material, washed with organic solvents, air dried, and rehydrated (Table I). CW#4 was used for measuring the previously published 2D and 3D spectra (Dick-Pérez et al., 2011; Wang et al., 2012). As we show in Supplemental Figure S1, the quantitative ^{13}C direct-polarization (DP) spectra of CW#4 have significantly higher pectin and glycoprotein signals than CW#1, indicating that the different seedlings and wall isolation methods used in the

Table I. *CW samples and preparation conditions*

Samples	Preparation Conditions
CW#1	Never-dried CW produced at Pennsylvania State University
CW#2	Lyophilized CW from the same batch as CW#1
CW#3	CW#2 rehydrated
CW#4	CW produced at Iowa State University, washed with organic solvents, air dried, and rehydrated
CW#5	CW#1 that was extracted with trans-1, 2-cyclohexanediaminetetraacetic acid (CDTA) and Na_2CO_3

two preparations caused different wall compositions. In 2D ^{13}C correlation spectra, both samples show cellulose-pectin correlation peaks (Supplemental Fig. S2), with CW#4 having moderately higher cross-peak intensities, consistent with its higher pectin content. Given the different wall compositions between CW#1 and CW#4, it is difficult to compare the effects of dehydration on wall structure; thus, we took the same batch of plant material as CW#1, dehydrated it to produce sample CW#2, and then rehydrated it to give sample CW#3 (Table I).

One-Dimensional ^{13}C- and ^{1}H-NMR Spectra of Never-Dried and Rehydrated CWs

We first examined the effects of lyophilization and rehydration on the structure and dynamics of wall polysaccharides by comparing the quantitative ^{13}C DP spectra of CW#1 to CW#3 (Fig. 1A). The never-dried CW#1 exhibits many sharp pectin peaks, such as the 53.7-ppm peak of methyl esters (full width at half maximum = 0.38 ppm), the 21.2-ppm peak of acetyl (0.81 ppm), the 17.6-ppm peak of Rha C6 (0.68 ppm), and the 79.7-ppm peak of GalA C4 and Rha C2 (0.70 ppm). Lyophilization (CW#2) severely broadened all these peaks, giving linewidths of approximately 8 ppm for the methyl ester peak and approximately 9 ppm for the acetyl group, indicating that water removal traps a broad distribution of conformations in these pectins. The loss of dynamic bulk water is confirmed by the ^{1}H spectrum (Fig. 1B). In comparison, the cellulose linewidths are less perturbed by drying: the 89-ppm interior cellulose C4 (iC4) peak increased its linewidth from 2.9 to 3.8 ppm, and the 65-ppm iC6 linewidth is also only moderately broadened by lyophilization. The relative stability of cellulose linewidths under dehydration is analogous to the insignificant broadening of cellulose peaks by freezing to cryogenic temperatures (Wang et al., 2013) and indicates that the conformational rigidity of cellulose microfibrils renders their NMR linewidths significantly independent of environmental changes.

When water is added back (CW#3), the ^{13}C DP spectrum is fully restored to the never-dried state, with similarly narrow pectin peaks. Thus, the conformations and hydrogen bonding of polysaccharides are reversible after rehydration, suggesting that the average polysaccharide structure in the dried CW is similar to that of the never-dried wall. The resumption of the narrow pectin linewidths also means that the broad conformational distribution of pectins in the dry wall is present in the never-dried wall, but they interconvert rapidly to give narrow linewidths at motionally averaged chemical shifts. In other words, polysaccharides with narrow linewidths due to dynamic averaging in the hydrated wall should manifest broad linewidths in the dehydrated wall.

To assess if polysaccharide mobilities are affected by hydration history, we measured ^{13}C cross-polarization (CP) spectra (Fig. 2A) and DP spectra with short recycle delays (Fig. 2B). The former preferentially enhance the signals of immobile polymers, while the

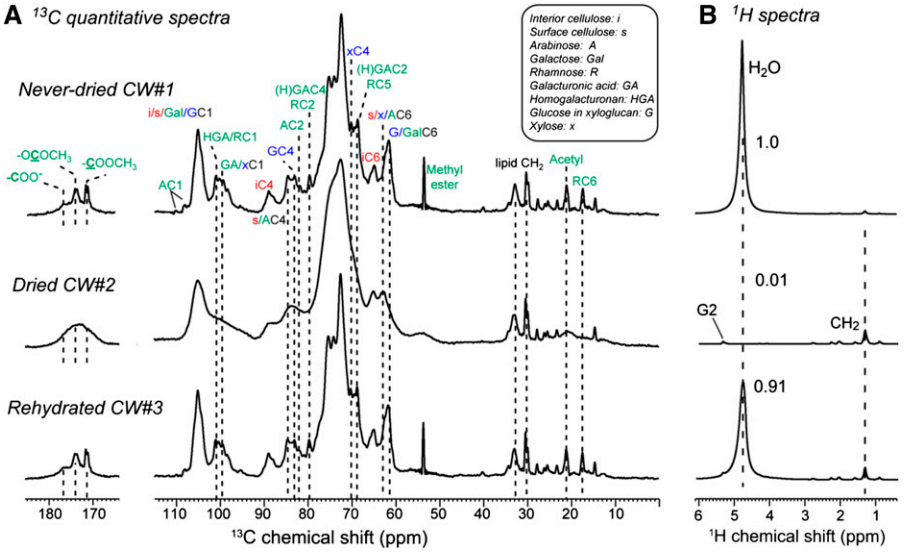

Figure 1. One-dimensional (1D) ^{13}C quantitative DP spectra (A) and ^{1}H spectra (B) of Arabidopsis CWs at 20°C under 9-kHz magic-angle spinning (MAS). A, ^{13}C spectra of never-dried CW#1, dried CW#2, and rehydrated CW#3. B, ^{1}H spectra, showing relative water intensities. Lyophilization removed all bulk water. The remaining ^{1}H signals in the dried wall result from lipids. The dried CW#2 exhibits severely broadened ^{13}C signals, but the linewidths are fully restored by rehydration in CW#3. The abbreviations for assignment are given.

latter preferentially detect mobile polysaccharides. The never-dried CW#1 and the rehydrated CW#3 have identical intensity distributions and linewidths in both the CP and DP spectra, indicating that these two samples have identical distributions of mobile and rigid molecules. For example, the short-recycle-delay DP spectra exhibit strong and narrow pectin carbonyl signals (165–180 ppm), arabinose C1 peak (108 ppm), GalA and Rha peaks (100, 80, 69, and 17 ppm), the methyl ester peak, and the acetyl peak.

Pectin-Cellulose Spatial Contacts from 2D ^{13}C-^{13}C Correlation NMR Spectra

To investigate whether the cellulose-pectin cross peaks reported previously (Wang et al., 2012) were caused by irreversible collapse of the polysaccharides during dehydration, we measured the 2D ^{1}H-driven ^{13}C-^{13}C spin diffusion (PDSD) spectrum of the never-dried CW#1 with a long mixing time of 1.5 s and compared it with the spectrum of the rehydrated CW#3 (Fig. 3). The CW#1 2D spectrum is remarkably similar to that of CW#3, with multiple cellulose-pectin cross peaks such as the iC6-HG/RC1 cross peak at 65 and 101 ppm and the iC4-HG/RC1 peak at 89 and 101 ppm. The 2D spectra have asymmetric cross-peak intensities around the diagonal: in the F1-F2 frequency dimensions, the cellulose-pectin cross peaks are higher than the pectin-cellulose cross peaks. This results from the higher CP intensities and slower T_1 relaxation of cellulose compared with pectins. Figure 3, C and D, shows key cellulose and pectin cross sections. In the 89- and 65-ppm cross sections of interior crystalline cellulose and the 84-ppm

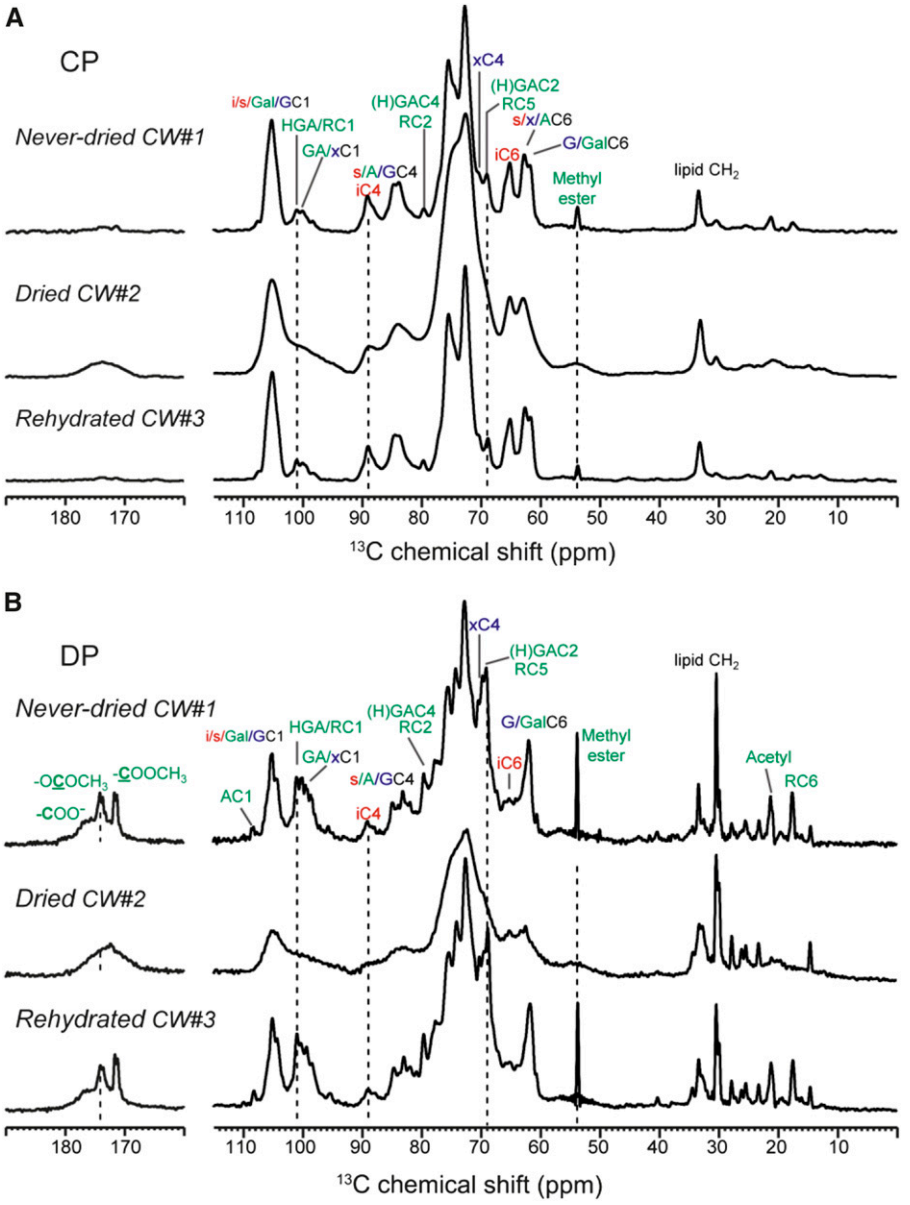

Figure 2. 1D ^{13}C CP (A) and DP (B) spectra of never-dried, dried, and rehydrated Arabidopsis primary walls at 20°C. The CP spectra selectively detect the signals of rigid polysaccharides, while the DP spectra with 2-s recycle delays preferentially detect the signals of dynamic polysaccharides. Rehydration fully restored polysaccharide linewidths to those seen for the never-dried CW#1.

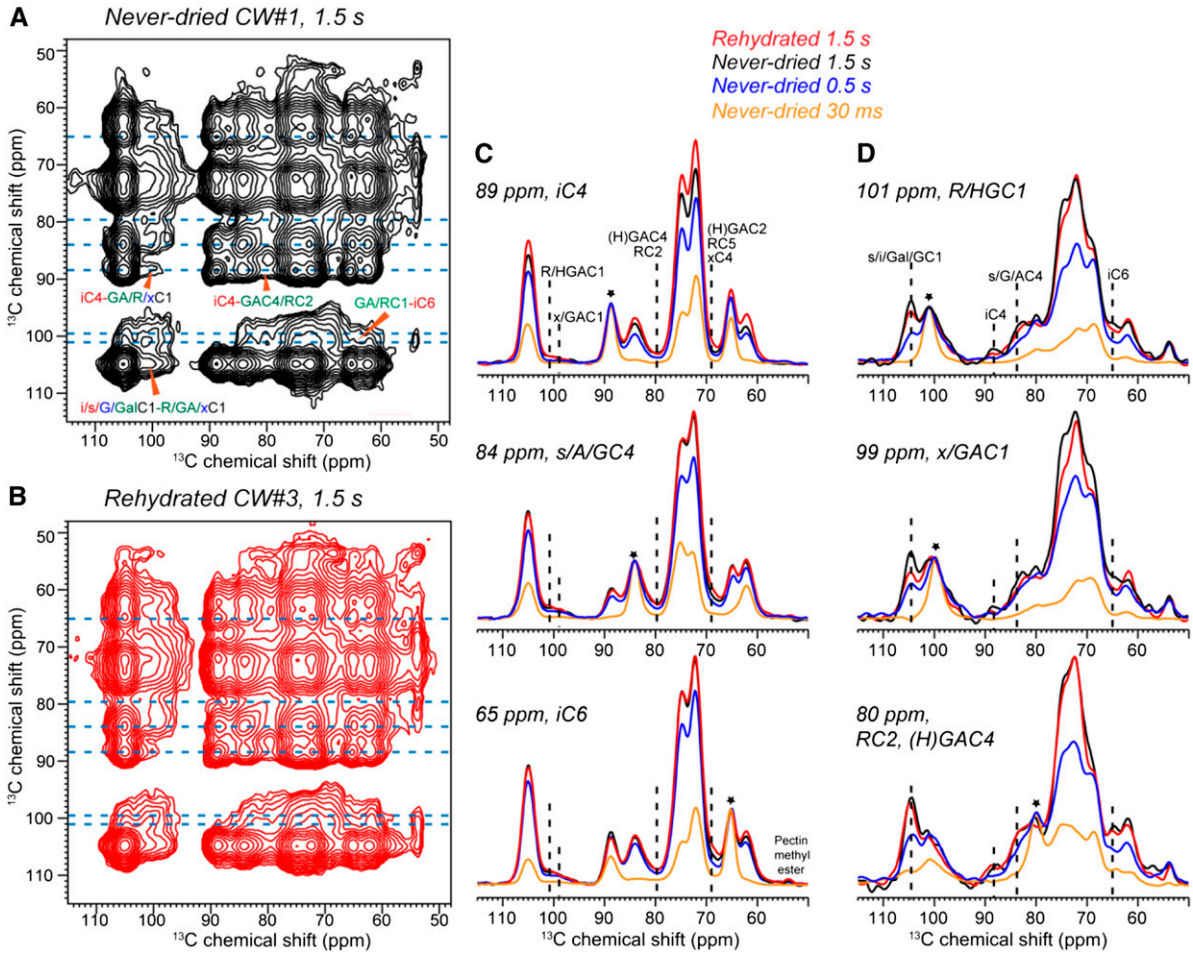

Figure 3. The 1.5-s 2D PDSD spectra of Arabidopsis CWs. A, Never-dried CW#1. B, Rehydrated CW#3. The spectra were measured at −20°C under 9-kHz MAS. C, Representative cellulose cross sections at various mixing times, normalized to the diagonal peaks (asterisks). D, Representative pectin cross sections. Intermolecular cellulose-pectin cross peaks are annotated. All cross peaks detected in the rehydrated CW#3 are also observed in the never-dried CW#1 with similar intensities, confirming that the close pectin-cellulose contact is intrinsic to the primary CW.

cross section of surface cellulose, XyG backbone, and Ara C4, unambiguous pectin cross peaks such as the 101-ppm peak of Rha and HG C1 and the 80-ppm peak of GalA C4 and Rha C2 are detected at mixing times longer than 500 ms. Cross peaks to mixtures of hemicellulose and pectin signals, such as the 99-ppm peak of Xyl and GalA C1 and the 69-ppm peak of GalA C2, Rha C5, and Xyl C4, are also observed. Conversely, the pectin cross sections exhibit well-resolved cross peaks to cellulose iC4 and iC6. The pectin-cellulose cross peaks have relatively high signal-to-noise ratios of 10 to 35. The never-dried CW#1 (black) and rehydrated CW#3 (red) show similar intensities for the pectin-cellulose cross peaks within experimental uncertainty, indicating that lyophilization and rehydration have negligible impact on the spatial proximities between the closely packed cellulose and pectins.

The 2D spectra in Figure 3 contain both intermolecular and intramolecular correlation signals. To better distinguish these two types of cross peaks, we measured a difference 2D spectrum (Wang et al., 2015) of CW#4 by subtracting two PDSD spectra with mixing times of 1 and 0.2 s. In the resulting difference spectrum (Fig. 4A), intermolecular cross peaks manifest as positive intensities while intramolecular cross peaks such as iC4-iC6 are removed. Both cellulose-pectin cross peaks and surface-interior cellulose cross peaks expected for the microfibril structure are clearly observed in the difference spectrum. Examples are the iC4-R/HGC1 (89 and 101 ppm), iC4-RC2/GAC4 (89 and 80 ppm), and iC6-R/HGC1 (65 and 101 ppm) peaks.

The 2D spectra in Figures 3 and 4 were measured at −20°C, where pectins were immobilized. To test whether the cross peaks indicative of close spatial contacts are an artifact of sample freezing, we measured 2D PDSD spectra at ambient temperature. Figure 5 shows that cellulose-pectin cross peaks remain at 20°C, albeit with slightly lower intensities than at low temperature due to the mobility of pectins at high temperature, which weakens the dipolar couplings

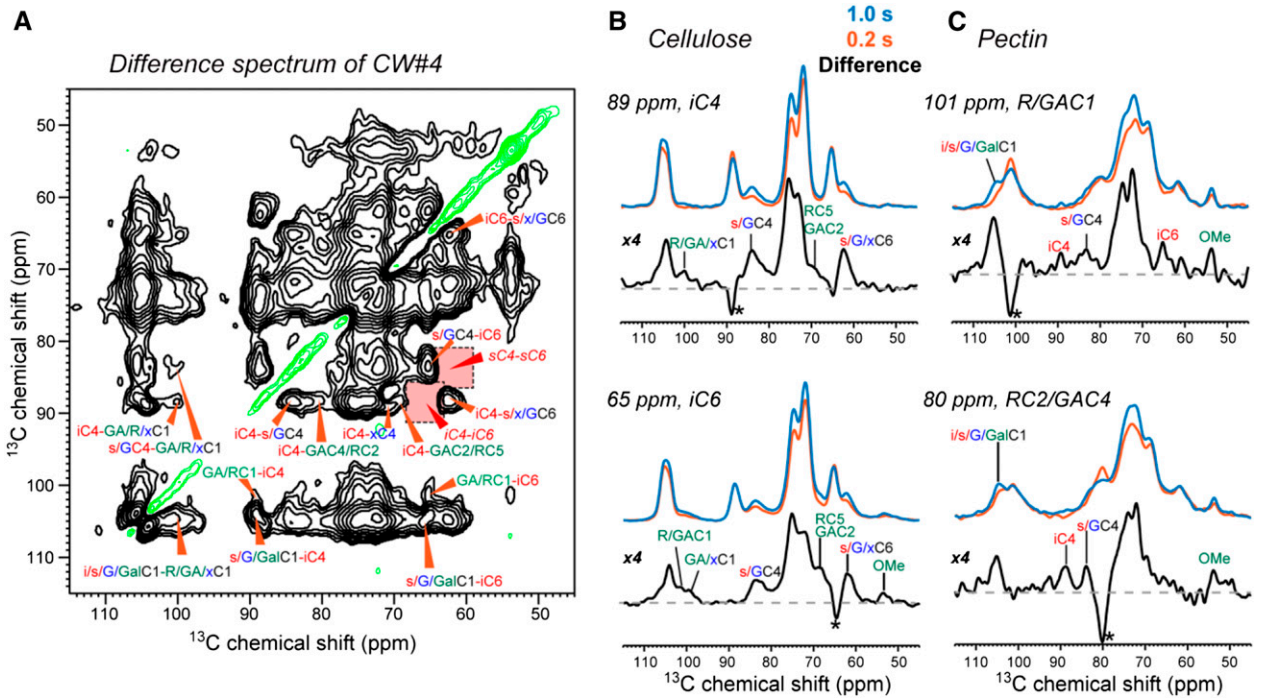

Figure 4. Difference 2D ^{13}C PDSD spectra of CW#4 with T_1 relaxation compensation to detect intermolecular correlations. A, Difference 2D spectrum between 1 s and 200 ms, measured with a constant z-period of 1.005 s, 8-kHz MAS, and at −20°C. Negative intensities along the diagonal are shown in green. Red shaded areas indicate intramolecular peaks that are present in the parent spectra, which are removed in the difference spectrum. B, Selected 1D cross sections of cellulose, showing the suppression of intramolecular cross peaks to better resolve the intermolecular cross peaks. Asterisks denote the diagonal peaks. C, Representative 1D cross sections of pectins.

that drive magnetization transfer. Thus, the close proximity between cellulose and pectins is present at ambient temperature, and the mild freezing in the SSNMR experiments does not perturb the wall structure.

Polysaccharide Mobilities in Never-Dried and Rehydrated CWs

To investigate whether dehydration and rehydration perturb polysaccharide mobility, we quantified the motional amplitudes and rates by measuring the ^{13}C-^{1}H dipolar order parameters (S_{CH}) and ^{13}C T_1 relaxation times. Supplemental Figure S3 shows that the C-H dipolar dephasing curves (Munowitz et al., 1981; Huster et al., 2001) are identical between the never-dried CW#1 and rehydrated CW#3 within experimental uncertainty. Fitting the dipolar decay curves yielded the S_{CH} (Fig. 6A). For both CWs, the S_{CH} values are highest for cellulose (approximately 0.9) and lowest for pectins (approximately 0.5), indicating that pectins have the largest motional amplitudes. No significant difference is observed between the two samples, indicating that rehydration resumes the same polysaccharide mobilities as the never-dried wall. Similarly, ^{13}C T_1 relaxation times (Fig. 6, B and C; Supplemental Fig. S4) are preserved between the never-dried and rehydrated walls, indicating that the nanosecond timescale motions are similar between the two samples.

The ^{13}C T_1 relaxation times can be used to determine the motional heterogeneity in each wall polymer, which cannot be determined in the ^{13}C-^{1}H dipolar chemical-shift experiment, which reports only the averaged bond order parameters. Cellulose generally exhibits single-exponential decays with long relaxation times of approximately 5 s, while matrix polysaccharides have double-exponential decays with equal contribution of a short component (approximately 0.3 s) and a long T_1 component (approximately 4.5 s; Tables II and III). iC6 also has a fast-relaxing component with low population (approximately 15%), which is likely caused by the influence from the surrounding pectins. The double-componential behavior is best seen in the pectin data, which show a distinct transition at approximately 0.5 s between the initial fast decay and the later slow decay. To assess if the matrix polysaccharides contain a third relaxation component that bridges the mobile and rigid portions, we fit the data using a triple-exponential function. However, the resulting fits show large uncertainties in either the T_1 values or the fractions or do not have sufficient differences in the T_1 values of the mobile and intermediate components (Supplemental Table S1). Thus, there is no compelling evidence for a third dynamic component in

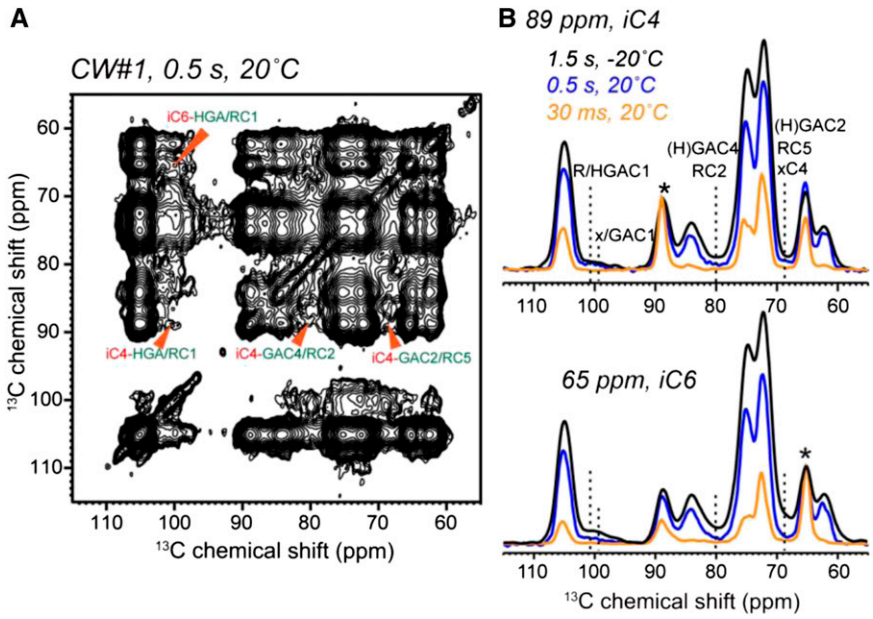

Figure 5. 2D PDSD spectra of never-dried CW#1 at ambient temperature, showing the retention of pectin-cellulose cross peaks. A, The 0.5-s PDSD spectrum at 20˚C. A few cellulose-pectin cross peaks are assigned. B, Representative cellulose cross sections from 2D spectra with mixing times of 30 ms and 0.5 s. The 1.5-s spectrum measured at −20˚C is superimposed for comparison. Pectin-cellulose cross peaks are present at high temperature, indicating that the intermolecular contacts detected at −20˚C are not due to freezing. The high-temperature cross peaks are lower than at low temperature due to the conformational dynamics of the pectins. Asterisks indicate diagonal peaks.

the matrix polysaccharides. These results suggest that the cellulose-contacting pectic units are rigidified by the microfibrils, while the pectic sugars that fill the interfibrillar space are dynamic. The main pectin signals detected here are RGI and HG backbones, because the galactan side-chain signals are difficult to resolve from the signals of the surface cellulose, xyloglucan, and the concentration of arabinan is low in this sample.

Water Interactions in the Never-Dried and Rehydrated Walls

To investigate water-polysaccharide interactions, we measured 2D ^{13}C-^{1}H heteronuclear correlation (HETCOR) spectra of never-dried CW#1 (Fig. 7A; Supplemental Fig. S5). In the absence of ^{1}H spin diffusion, only polysaccharide self-correlation peaks are seen. With a ^{1}H spin diffusion mixing time of 1 ms, water cross peaks are observed for most polysaccharides at a ^{1}H chemical shift of 4.7 ppm. Since some polysaccharide protons have similar chemical shifts to the water proton, we further conducted a dipolar-filtered medium- and long-distance (MELODI)-HETCOR experiment (Yao et al., 2001; Li et al., 2010) to remove the one-bond ^{13}C-^{1}H cross peaks by means of their strong ^{13}C-^{1}H dipolar coupling. In the absence of ^{1}H spin diffusion, the MELODI-HETCOR spectrum (Fig. 7B) suppressed most polysaccharide signals except for a weak methyl ester peak at 3.8 ppm, as expected. With 1 ms of ^{1}H spin diffusion, multiple cross peaks at the ^{1}H chemical shift of 4.7 ppm are detected, while other cross peaks are suppressed (Fig. 7C). Thus, the 4.7-ppm ^{1}H cross section indeed corresponds to water-polysaccharide correlations. Comparison of the HETCOR and MELODI-HETCOR spectra shows that the water-edited spectrum preferentially enhances the pectin signals (Fig. 7D), indicating that pectins constitute the majority of the hydrated polysaccharides, in excellent agreement with the results of a recent hydration study by ^{1}H polarization transfer NMR (White et al., 2014). Both surface cellulose and interior cellulose (e.g. the 89-ppm C4 peak) show water cross peaks. Due to the 1-ms ^{1}H spin diffusion period, this polarization most likely originates from water on the surface rather than in the interior of the microfibril. Interestingly, the water-correlated iC4 peak has half the linewidth as the cellulose C4 peak in the HETCOR (Fig. 7E). Since the HETCOR spectrum exhibits all interior cellulose signals due to the presence of polysaccharide protons that resonate between 4.5 and 5 ppm (Kono et al., 2003), whereas the MELODI-HETCOR spectrum detects only water-contacting cellulose, the line narrowing indicates that the water-proximal interior cellulose chains adopt a subset of conformations that are present among all the glucan chains in the microfibril.

The rehydrated CW#3 shows similar HETCOR and MELODI-HETCOR spectra (Supplemental Fig. S6) to the never-dried CW#1, except that the water-contacting pectins have 10% to 25% lower intensities when normalized by the iC4 peak (Supplemental Fig. S7), indicating that the pectin-water association is slightly reduced in the rehydrated CW.

Investigation of Molecular Crowding Using HG-Extracted CW

To probe whether the cellulose-pectin spatial contacts in the never-dried wall result from nonspecific molecular crowding or specific interactions, we investigated a partially HG-extracted never-dried CW (CW#5). Previous monosaccharide analysis indicated that this sample contains approximately 40% less HG

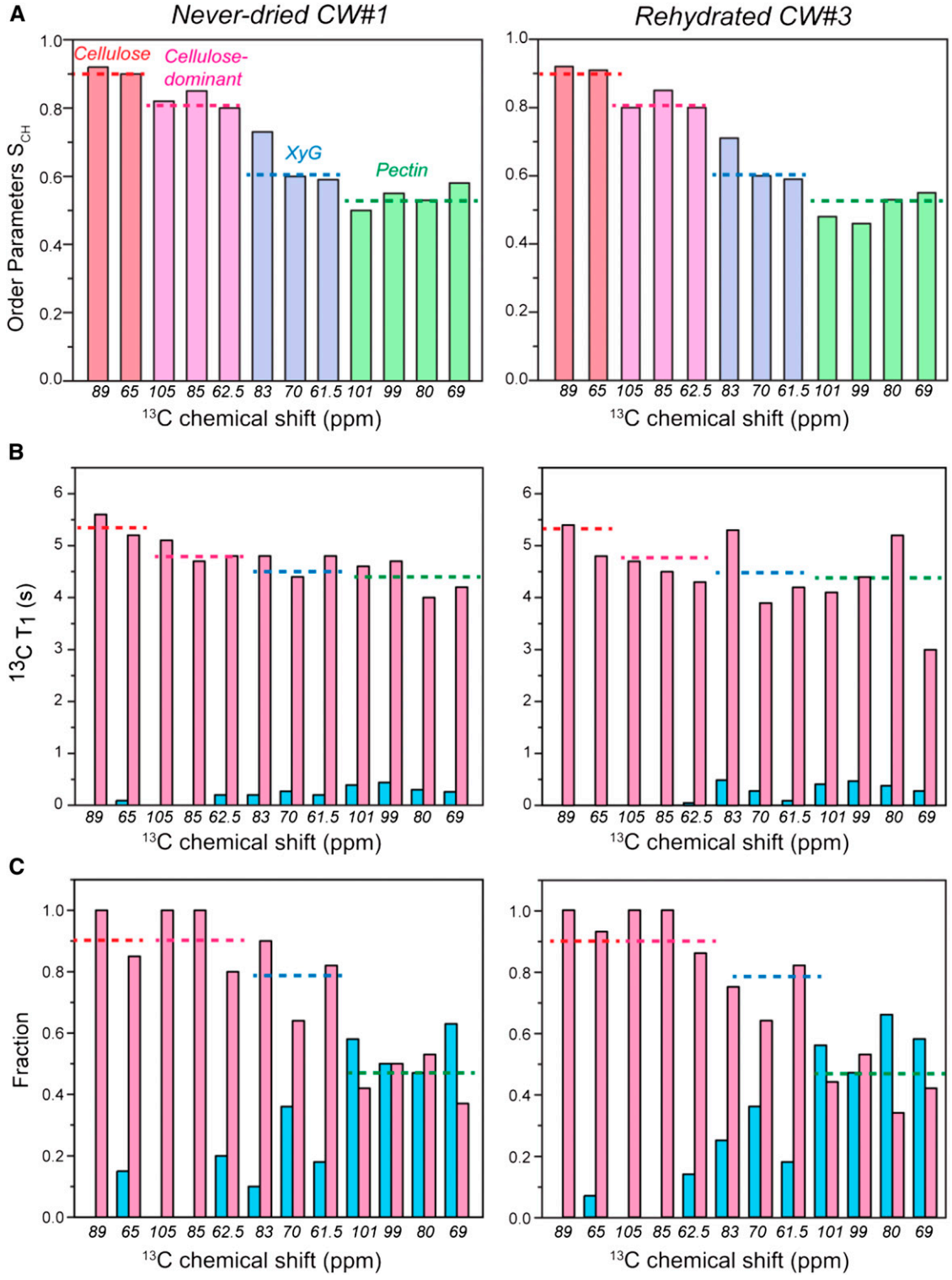

Figure 6. Comparison of polysaccharide mobility between the never-dried CW#1 (left) and the rehydrated CW#3 (right). A, S_{CH}, obtained from a quantitative ^{13}C-^{1}H dipolar chemical-shift spectrum measured at 20°C. The S_{CH} values are very similar between the two samples, indicating similar motional amplitudes. B, ^{13}C T_1 relaxation times. Matrix polysaccharides exhibit a short (cyan) and a long (magenta) T_1 component, which likely correspond to cellulose-unbound and -bound fractions. C, Fractions of the short and long T_1 components. The never-dried and rehydrated walls have similar T_1 distributions.

Table II. *^{13}C T_1 relaxation times of never-dried CW#1*

The single and double exponential functions used to fit the data are $I(t) = e^{-t/T_{1b}}$ and $I(t) = ae^{-t/T_{1a}} + be^{-t/T_{1b}}$, where $b = 1 - a$. –, Unidentified.

Assignment	δ_C	*a* (Mobile)	*b* (Rigid)	T_{1a}	T_{1b}
	ppm			*s*	
i/s/G/GalC1	105.0	–	1	–	5.1 ± 0.1
HG/RC1	101.0	0.58 ± 0.01	0.42 ± 0.01	0.39 ± 0.01	4.6 ± 0.2
x/GAC1	99.7	0.50 ± 0.02	0.50 ± 0.02	0.44 ± 0.03	4.7 ± 0.2
iC4	89.0	–	1	–	5.6 ± 0.1
s/GC4	84.5	–	1	–	4.7 ± 0.1
GC4	83.0	0.10 ± 0.01	0.90 ± 0.01	0.20 ± 0.05	4.8 ± 0.1
RC2/(H)GAC4	79.9	0.47 ± 0.03	0.53 ± 0.03	0.30 ± 0.04	4.0 ± 0.3
xC4	70.4	0.36 ± 0.02	0.64 ± 0.02	0.27 ± 0.03	4.4 ± 0.2
(H)GAC2/RC5	69.0	0.63 ± 0.02	0.37 ± 0.02	0.26 ± 0.02	4.2 ± 0.3
iC6	65.2	0.15 ± 0.01	0.85 ± 0.01	0.09 ± 0.02	5.2 ± 0.1
sC6,x/AC5	62.6	0.20 ± 0.05	0.80 ± 0.05	0.13 ± 0.01	4.9 ± 0.1
G/GalC6	61.7	0.18 ± 0.01	0.82 ± 0.01	0.20 ± 0.03	4.8 ± 0.1

due to extraction by CDTA and sodium carbonate (White et al., 2014). Figure 8 shows the 1-s 2D PDSD spectrum of this HG-reduced CW. Cellulose-pectin cross peaks such as GA/R/xC1-iC4 at 100 and 89 ppm remain in the 2D spectrum. Representative cellulose and pectin cross sections show that the cellulose-pectin cross-peak intensities are similar between the intact and extracted walls, indicating that the removed HG does not contact cellulose in the original wall. Thus, pectin-cellulose spatial contacts are not caused by molecular crowding but by specific interactions, which may involve pectin entrapment within and between cellulose microfibrils.

DISCUSSION

Our recent SSNMR studies of intact Arabidopsis primary CWs (Dick-Pérez et al., 2011, 2012; Wang et al., 2012, 2013; White et al., 2014) led to the proposal of a single-network model of wall polysaccharides, which differs from the prevailing CW model in which pectins do not form stable interactions with cellulose but constitute a gel-like milieu that embeds a cellulose-xyloglucan network and interacts with cellulose only via polymer entanglements (Carpita and Gibeaut, 1993; Cosgrove, 2001, 2005). The current study was designed to further test the authenticity of cellulose-pectin spatial contacts and gain insight into the structural details of such contacts. Are cellulose-pectin contacts artifacts of transient dehydration during CW preparation? Do these contacts result from molecular crowding or specific binding that have escaped previous studies? The present SSNMR data show that quantitative ^{13}C spectral intensities, ^{13}C linewidths, 2D correlation peaks, and polysaccharide mobilities are indistinguishable between the never-dried and rehydrated walls, thus demonstrating that lyophilization followed by rehydration restores the wall polysaccharides to their original structure and dynamics. Dehydration did not cause irreversible changes in the wall polymer interactions. We propose that the reversibility of CW structure and dynamics upon rehydration is due to two factors: the rigidity of cellulose microfibrils, which provide a robust scaffold to the CW, and the ease of the charged, hydroxyl-rich, and Ca^{2+}-chelated matrix polysaccharides to associate with water (White et al., 2014).

Four pieces of experimental evidence support the existence of specific cellulose-pectin binding in the never-dried CW. First, pectin-cellulose cross peaks largely

Table III. *^{13}C T_1 relaxation times of Arabidopsis CW#3*

–, Unidentified.

Assignment	δ_C	*a* (Mobile)	*b* (Rigid)	T_{1a}	T_{1b}
	ppm			*s*	
i/s/G/GalC1	105.0	–	1	–	4.7 ± 0.1
HG/RC1	101.0	0.56 ± 0.01	0.44 ± 0.01	0.41 ± 0.01	4.1 ± 0.1
x/GAC1	99.7	0.47 ± 0.03	0.53 ± 0.03	0.47 ± 0.04	4.4 ± 0.3
iC4	89.0	–	1	–	5.4 ± 0.1
s/GC4	84.5	–	1	–	4.5 ± 0.1
GC4	83.0	0.25 ± 0.02	0.75 ± 0.02	0.49 ± 0.05	5.3 ± 0.2
RC2/(H)GAC4	79.9	0.66 ± 0.02	0.34 ± 0.02	0.38 ± 0.02	5.2 ± 0.3
xC4	70.4	0.36 ± 0.02	0.64 ± 0.02	0.28 ± 0.03	3.9 ± 0.2
(H)GAC2/RC5	69.0	0.58 ± 0.03	0.42 ± 0.03	0.28 ± 0.03	3.0 ± 0.3
iC6	65.2	0.07 ± 0.01	0.93 ± 0.01	0.01 ± 2.27	4.8 ± 0.1
sC6,x/AC5	62.6	0.14 ± 0.05	0.86 ± 0.05	0.05 ± 0.02	4.3 ± 0.1
G/GalC6	61.7	0.18 ± 0.01	0.82 ± 0.01	0.09 ± 0.02	4.2 ± 0.1

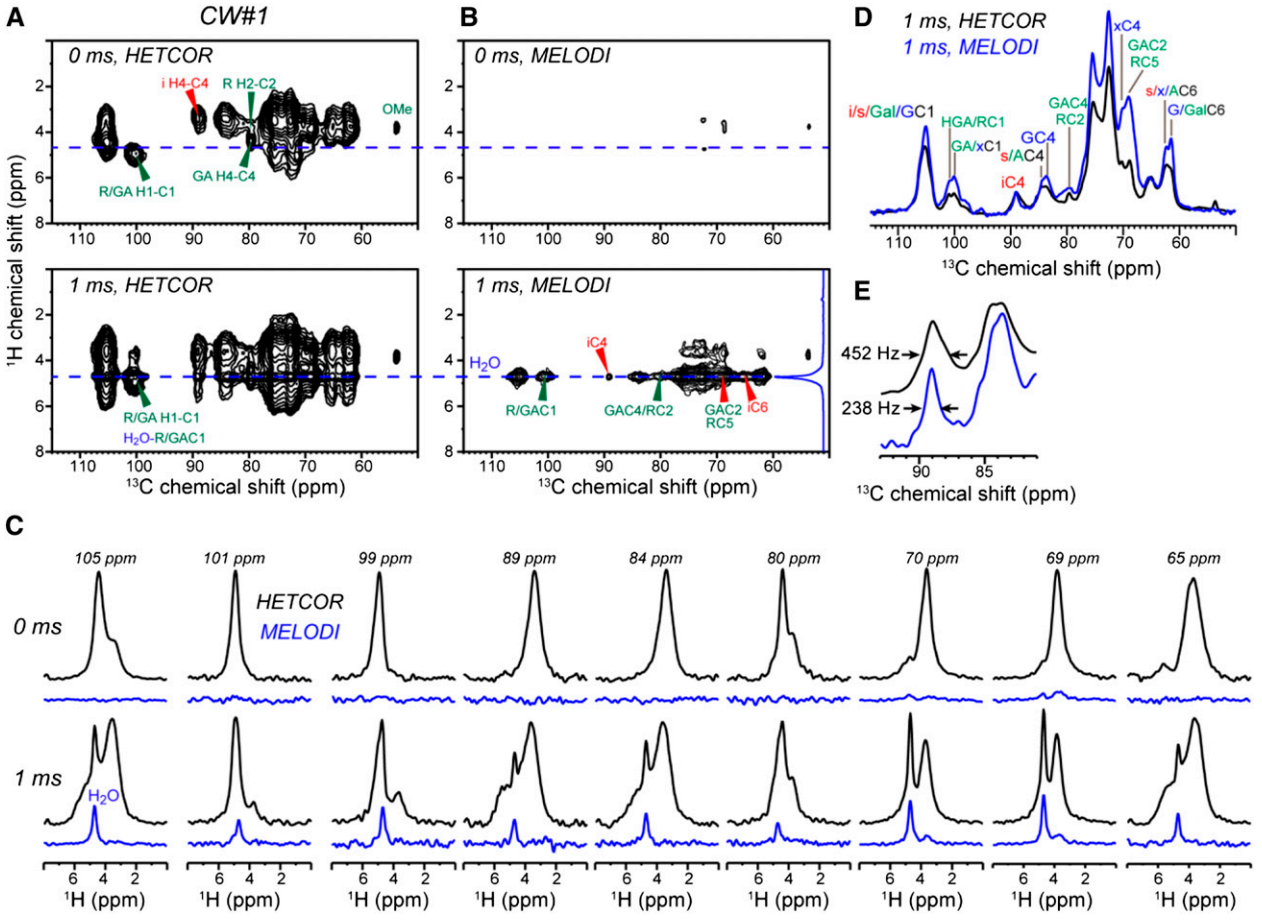

Figure 7. 2D ^{13}C-^{1}H HETCOR spectra of never-dried CW#1 to probe water-polysaccharide interactions. The spectra were measured at 20°C under 14.8-kHz MAS. A, 2D HETCOR spectrum without and with ^{1}H spin diffusion. B, MELODI-HETCOR spectrum without and with spin diffusion. C, Representative ^{1}H cross sections from the HETCOR (black) and MELODI-HETCOR (blue) spectra with 0- and 1-ms ^{1}H spin diffusion. D, ^{1}H projection of the 1-ms HETCOR spectrum (black) compared with the water ^{1}H cross section of the 1-ms MELODI-HETCOR spectrum (blue). The water cross section shows higher pectin intensities. E, Expanded cellulose region of D. The water-contacting cellulose has narrower linewidth than the average cellulose.

remain even after 40% of the HG has been extracted; thus, molecular crowding is not the chief reason for the cellulose-pectin spatial contact. This result also means that about half of the HG does not participate in cellulose binding; thus, the main cellulose-binding pectins are either RGI or the remaining portion of HG or both. Second, a recent hydration study showed that the removal of Ca^{2+} ions, which cross link HG, slows down water ^{1}H magnetization transfer to both cellulose and pectins instead of only pectins (White et al., 2014), indicating that pectins are in intimate contact with cellulose. Third, in the never-dried wall, pectins show a long ^{13}C T_1 component of approximately 4.5 s, comparable to the T_1 of cellulose (approximately 5 s; Tables II and III). This rigid fraction represents approximately 50% of pectins, similar to the fraction of HG that cannot be extracted by CDTA and sodium carbonate. These results strongly suggest that the rigid pectins are what remain in the wall, bound to cellulose. Indeed, a previous SSNMR study of a similarly depectinated Arabidopsis CW (Dick-Perez et al., 2012) showed significant increases in the ^{13}C T_1 relaxation time and ^{1}H rotation-frame longitudinal relaxation time, confirming that the unextracted pectins are more rigid. Fourth, the cellulose-pectin cross peaks are observed at both low and high temperatures; thus, they are not caused by freezing-induced alterations of polymer packing. The preservation of the cross peaks at high temperature further verifies the conclusion that the more rigid fraction of pectins is responsible for the close contact with cellulose.

Taken together, these spectroscopic data indicate that part of HG and the majority of RGI have significant and specific contacts with cellulose microfibrils. We hypothesize that the pectins may be entrapped inside or between cellulose microfibrils, which may occur during CW biosynthesis: pectins, secreted from the Golgi, may interact with the plasma membrane-synthesized glucan chains when both are transported to the CW.

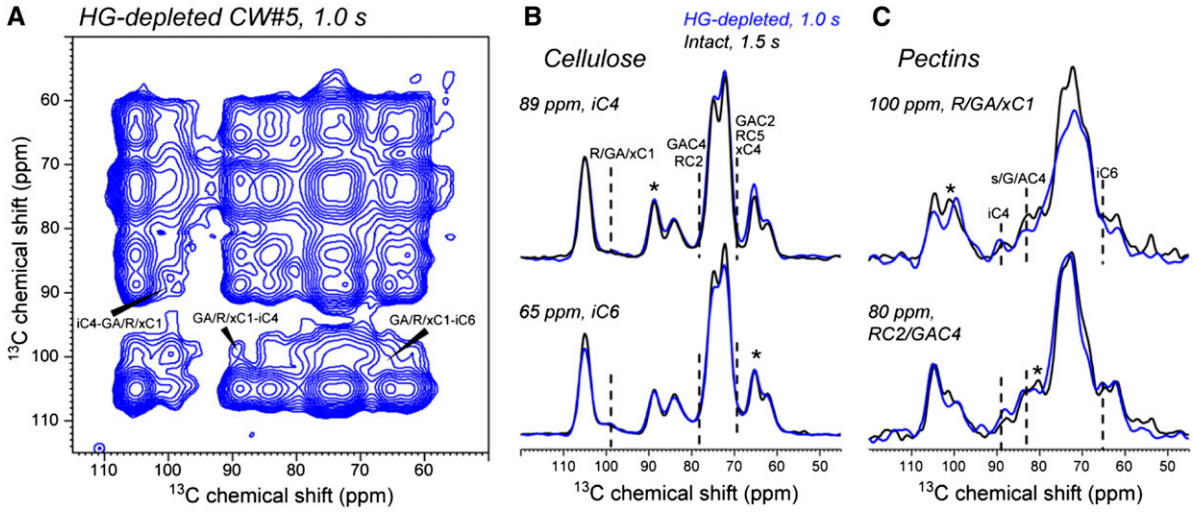

Figure 8. Observation of cellulose-pectin cross peaks in HG-reduced CW#5. A, 2D PDSD spectrum with 1-s ^{13}C spin diffusion. Some of the cellulose-pectin cross peaks are assigned. B, Comparison of the main cellulose cross sections between CW#5 (blue) and CW#1 (black). C, Comparison of the main pectin cross sections between CW#5 and CW#1. The HG-reduced wall shows similar cellulose-pectin cross-peak intensities to the intact wall. The two spectra were measured at about −20°C under 9-kHz MAS.

The persistence of hydration- and temperature-independent pectin-cellulose cross peaks in multiple Arabidopsis primary wall samples raises the question of why in vitro binding assays found only weak association between these two polysaccharides (Chanliaud and Gidley, 1999; Zykwinska et al., 2007, 2008). Pectins bind up to approximately 10 μg mg^{-1} cellulose, compared with xyloglucan, which binds cellulose to approximately 120 μg mg^{-1} cellulose. An examination of the protocols for the binding studies suggests several possible reasons for this apparent discrepancy. First, the binding assays used polysaccharides that were extracted by strong acid and alkali solutions of 0.5 to 6 M in concentration, at temperatures of 40°C to 80°C, and with up to 95% ethanol. The strong chemical extraction procedures perturb the conformation, esterification, and methylation of the polysaccharides and may irreversibly remove important intermolecular interactions. For example, in one study, the extracted sugar beet (*Beta vulgaris*) pectin used for cellulose binding is predominantly HG and contains little Rha. Since neutral arabinan and galactan are known to have higher affinity to cellulose than anionic galacturonic acids, the reduced amount of RGI in the extracted pectins could reduce the measured binding level. Indeed, comparison of commercial pectins with a few neutral side chains and mildly treated natural pectins in plant CWs that preserve the neutral side chains shows higher cellulose binding for the latter (Zykwinska et al., 2005).

Second, some binding assays used bacterial cellulose, whose structure differs from that of plant cellulose (Chanliaud and Gidley, 1999; Zykwinska et al., 2005). Bacterial cellulose is rich in the I_α allomorph, while the secondary walls of higher plants mainly contain the I_β allomorph (Atalla and Vanderhart, 1984), whose conformations and hydrogen-bonding patterns differ from those of the I_α allomorph (Nishiyama et al., 2002, 2003). In Arabidopsis leaves, the cellulose ^{13}C signals indicate the presence of both I_α and I_β allomorphs, with slightly higher I_β contents (Newman et al., 1996). The detailed structures of primary wall microfibrils are still unknown, but in silico results suggest that cellulose chains in small microfibrils differ from those in extended crystalline phases in terms of chain tilts and various dihedral angles (Oehme et al., 2015). In addition, commercial Avicel microcrystalline cellulose has been shown to bind pectins more weakly than plant CW cellulose (Zykwinska et al., 2005), possibly due to its decreased surface area. Thus, the use of cellulose with different origins from the plant CW calls for caution in interpreting the results of in vitro binding assays.

Third, in vitro binding assays generally report much lower binding than in vitro extraction assays (Ryden and Selvendran, 1990; Oehme et al., 2015), which also report the strength of the intermolecular interactions. This discrepancy also exists for xyloglucan, where both the amount and strength of binding to cellulose are much less for in vitro assays than is the case in vivo assays in plant CWs (Hayashi et al., 1987). On the molecular level, this discrepancy between the bottom-up and top-down assays is conceivable because absorption studies limit possible binding to the cellulose surface, while polysaccharide entrapment within or between microfibrils can occur during CW biosynthesis. It is known that primary wall cellulose has a lower crystallinity than the crystallinity of cellulose in synthetic composites, further suggesting that in vitro binding assays cannot reproduce the complexity of the polysaccharide interactions in the native wall. Taken

together, these considerations suggest that the cellulose-pectin NMR cross peaks observed in never-dried walls at ambient temperature are more authentic indicators of the wall structure than in vitro assays of cellulose-pectin composite formation.

While this study demonstrates the existence of cellulose-pectin close contacts in the never-dried primary wall, the nature of this intermolecular interaction requires further investigations. One question is whether RGI or HG is more responsible for interacting with cellulose. At present, it is difficult to fully resolve the HG and RGI ^{13}C chemical shifts. Polysaccharide-specific isotopic labeling and/or mutant plants deficient in one of the two pectins would be desirable for answering this question. It is also unclear whether pectins can interact with multiple microfibrils at the same time, which is a prerequisite for the load-bearing function in both the tethered-network and the hotspots models.

MATERIALS AND METHODS

Plant Material

Never-dried Arabidopsis (*Arabidopsis thaliana*) primary CWs (CW#1) were prepared and ^{13}C labeled at Pennsylvania State University as described recently (White et al., 2014). Briefly, Arabidopsis seedlings were harvested after dark growth for 14 d in liquid culture containing ^{13}C-labeled Glc as the sole carbon source. The seedlings were frozen, ground in liquid nitrogen, and washed with 1.5% (w/v) SDS for 3 h to solubilize cell membranes and proteins and to inactivate endogenous wall-degrading enzymes (Zablackis et al., 1995; Gibeaut et al., 2005). The material was washed extensively in water, incubated with α-amylase (5,000 units in 30 mL) from porcine pancreas (Sigma-Aldrich) in sodium MES buffer (pH 6.8) to remove starch, and then digested with Pronase (Roche Life Sciences; 200 units, 5 mg in 20 mL) in sodium MES buffer (pH 7.5) to digest proteins. The Pronase was finally inactivated by incubating the sample with shaking in 1.5% (w/v) SDS at room temperature for 1 h. A total of 0.02% (w/v) NaN_3 was used in all solutions to inhibit microbial growth. Bulk water was removed by centrifugation (White et al., 2014). This sample preparation procedure avoided extensive washes with organic solvents and air drying, which were used in an earlier sample prepared at Iowa State University (CW#4; Dick-Pérez et al., 2011). Walls that have been frozen, thawed, and washed with detergents retain their original mechanical characteristics as well as their microscopic appearance as seen by atomic force microscopy (Zhang et al., 2014), so the molecular interactions are believed to be largely unperturbed by such treatment. Approximately 60 mg of the never-dried CW#1 was packed into 4-mm MAS rotors for SSNMR experiments.

As controls, another 60 mg of the same batch of never-dried wall was packed into an MAS rotor and lyophilized for 1 d. A total of 47 mg of water was removed, and a ^1H-NMR spectrum confirmed the loss of bulk water. ^{13}C spectra of this dehydrated CW#2 sample were measured. Subsequently, an equivalent amount of water was added back to this dehydrated sample and mixed homogenously for a few minutes to produce CW#3. The dried wall absorbed water readily.

We also remeasured the organic solvent-washed, air-dried, and rehydrated CW#4. This sample was used to obtain the previously reported cellulose-pectin cross peaks (Dick-Pérez et al., 2011; Wang et al., 2012). We measured relaxation-compensated difference 2D spectra on this CW#4 to verify the previous results and to compare with the never-dried CW#1.

A partially depectinated sample, CW#5, was prepared by treating the never-dried CW#1 with 50 mM CDTA for 16 h at 25°C with three changes of solution to chelate Ca^{2+} ions and solubilize HG, then with 50 mM sodium carbonate with 20 mM $NaBH_4$ (to minimize polysaccharide degradation) at 22°C for 16 h with three changes of solution to neutralize galacturonic acid and hydrolyze methyl esters to carboxylate ions. Quantitative ^{13}C-NMR spectra show that approximately 40% of HG was removed by this protocol, while the majority of RGI (approximately 95%) remained (White et al., 2014). This HG-depleted sample was measured to compare with the never-dried CW#1.

Solid-State NMR Experiments

Most SSNMR experiments were conducted on a Bruker Avance II 600-MHz spectrometer (14.1 Tesla) using a 4-mm MAS probe. ^{13}C-^1H HETCOR spectra were measured on a Bruker 900-MHz spectrometer (21.1 Tesla) using a 3.2-mm MAS probe. PDSD experiments with CW#5 at −18°C and CW#1 at 20°C were conducted on a Bruker Avance III 400-MHz spectrometer using a 4-mm MAS probe. Typical radio frequency field strengths were 50 to 83 kHz for ^1H and 40 to 50 kHz for ^{13}C. ^{13}C chemical shifts were externally referenced to the adamantane CH_2 signal at 38.48 ppm on the tetramethylsilane scale.

1D ^{13}C MAS spectra were measured at 20°C under 9-kHz MAS using either DP or CP to create the initial ^{13}C magnetization. DP experiments were conducted with a long recycle delay of 25 s to obtain quantitative spectra or a short recycle delay of 2 s to selectively detect dynamic polysaccharides, while CP experiments were used to preferentially detect rigid polysaccharide signals.

2D ^{13}C-^{13}C PDSD experiments were conducted on the never-dried CW#1, rehydrated CW#3, and HG-depleted CW#5 with mixing times of 1 to 1.5 s to detect long-range (approximately 1 nm) intermolecular correlations under varying hydration histories and polysaccharide densities. These spectra were measured at −20°C, where both pectins and cellulose were immobilized, which facilitates magnetization transfer (Wang et al., 2012). The 2D experiments were also conducted at 20°C on CW#1 with mixing times of 5 to 500 ms to verify whether the intermolecular contacts also exist at ambient temperature. The relaxation-compensated PDSD experiment was conducted on CW#4 to obtain clean difference spectra showing only intermolecular cross peaks (Wang et al., 2015). The experiment inserts a z-filter before the evolution period, so that the sum of the z-filter and the spin diffusion mixing time is a constant value of 1.005 s. Two parent spectra, with mixing times of 1 s and 200 ms, were measured, and a difference spectrum was obtained by subtracting the 200-ms spectrum after scaling by 0.83 from the 1-s spectrum.

The amplitudes and rates of polysaccharide motion were measured on the never-dried CW#1 and rehydrated CW#3. ^{13}C-^1H dipolar chemical-shift correlation experiments (Munowitz et al., 1981) were conducted at 20°C under 7-kHz MAS to measure S_{CH}. The frequency-switched Lee-Goldburg sequence (Bielecki et al., 1989) was used for ^1H homonuclear decoupling. This theoretical scaling factor of 0.577 was verified using the model peptide formyl-Met-Leu-Phe (Rienstra et al., 2002). The ratio of the true coupling to the rigid-limit value of 22.7 kHz gives the S_{CH} (Supplemental Fig. S3). ^{13}C T_1 relaxation times were measured using a z-filter sequence (Torchia, 1978) at 20°C under 9-kHz MAS. Most relaxation decays are well fit by a double exponential function (Tables II and III; Supplemental Fig. S4).

2D ^1H-^{13}C HETCOR experiments were carried out at 20°C under 14.8-kHz MAS on a 900-MHz spectrometer. For the Lee-Goldburg HETCOR experiment, ^1H homonuclear decoupling was achieved using the frequency-switched Lee-Goldburg sequence with a ^1H transverse field strength of 80 kHz during t_1 evolution, followed by a mixing period for ^1H spin diffusion. The ^1H magnetization was transferred to ^{13}C by 300 μs of Lee-Goldburg CP (van Rossum et al., 2000). The ^1H chemical shift was calibrated using formyl-Met-Leu-Phe (Li et al., 2010). To detect unambiguous polysaccharide-water cross peaks, we also measured dipolar-edited MELODI HETCOR spectra (Yao and Hong, 2001; Yao et al., 2001). Eight rotor periods of C-H dipolar dephasing were used before the ^1H t_1 evolution period to dephase the ^1H signals of ^{13}C-labeled polysaccharides and retain only the water ^1H cross peaks to the polysaccharide ^{13}C signals. The 180° pulse lengths were 10 μs for ^{13}C and 6.25 μs for ^1H. Hartman-Hahn CP with 300 μs contact time was used for the MELODI-HETCOR experiments.

Supplemental Data

The following supplemental materials are available.

Supplemental Figure S1. 1D ^{13}C MAS spectra of never-dried CW#1 and rehydrated CW#4.

Supplemental Figure S2. 2D ^{13}C spectra of never-dried CW#1 and rehydrated CW#4.

Supplemental Figure S3. C-H dipolar dephasing curves of CW#1 and CW#3.

Supplemental Figure S4. ^{13}C T_1 relaxation curves of never-dried CW#1 and rehydrated CW#3.

Supplemental Figure S5. Full 2D HETCOR spectrum of never-dried CW#1.

Supplemental Figure S6. ^{13}C-^{1}H HETCOR spectra of rehydrated CW#3.

Supplemental Figure S7. Water cross sections of MELODI-HETCOR spectra of CW#1 and CW#3.

Supplemental Table S1. Triple-exponential fitting of ^{13}C T_1 relaxation data.

Received May 4, 2015; accepted May 29, 2015; published June 2, 2015.

LITERATURE CITED

Albersheim P, Darvill A, Roberts K, Sederoff R, Staehelin A (2011) Plant Cell Walls. Garland Science, New York

Atalla RH, Vanderhart DL (1984) Native cellulose: a composite of two distinct crystalline forms. Science **223:** 283–285

Bielecki A, Kolbert AC, Levitt MH (1989) Frequency-switched pulse sequences: homonuclear decoupling and dilute spin NMR in solids. Chem Phys Lett **155:** 341–346

Caffall KH, Mohnen D (2009) The structure, function, and biosynthesis of plant cell wall pectic polysaccharides. Carbohydr Res **344:** 1879–1900

Carpita NC, Gibeaut DM (1993) Structural models of primary cell walls in flowering plants: consistency of molecular structure with the physical properties of the walls during growth. Plant J **3:** 1–30

Chanliaud E, Gidley MJ (1999) In vitro synthesis and properties of pectin/Acetobacter xylinus cellulose composites. Plant J **20:** 25–35

Cornuault V, Manfield IW, Ralet MC, Knox JP (2014) Epitope detection chromatography: a method to dissect the structural heterogeneity and inter-connections of plant cell-wall matrix glycans. Plant J **78:** 715–722

Cosgrove DJ (2001) Wall structure and wall loosening: a look backwards and forwards. Plant Physiol **125:** 131–134

Cosgrove DJ (2005) Growth of the plant cell wall. Nat Rev Mol Cell Biol **6:** 850–861

Cosgrove DJ (2014) Re-constructing our models of cellulose and primary cell wall assembly. Curr Opin Plant Biol **22:** 122–131

Dick-Perez M, Wang T, Salazar A, Zabotina OA, Hong M (2012) Multidimensional solid-state NMR studies of the structure and dynamics of pectic polysaccharides in uniformly ^{13}C-labeled *Arabidopsis* primary cell walls. Magn Reson Chem **50:** 539–550

Dick-Pérez M, Zhang Y, Hayes J, Salazar A, Zabotina OA, Hong M (2011) Structure and interactions of plant cell-wall polysaccharides by two- and three-dimensional magic-angle-spinning solid-state NMR. Biochemistry **50:** 989–1000

Fleischer A, O'Neill MA, Ehwald R (1999) The pore size of non-graminaceous plant cell walls is rapidly decreased by borate ester cross-linking of the pectic polysaccharide rhamnogalacturonan II. Plant Physiol **121:** 829–838

Foster TJ, Ablett S, McCann MC, Gidley MJ (1996) Mobility-resolved C-13-NMR spectroscopy of primary plant cell walls. Biopolymers **39:** 51–66

Gibeaut DM, Pauly M, Bacic A, Fincher GB (2005) Changes in cell wall polysaccharides in developing barley (Hordeum vulgare) coleoptiles. Planta **221:** 729–738

Goodneratne J, Needs PW, Ryden P, Selvendran RR (1994) Structural features of cell wall polysaccharides from the cotyledons of mung bean Vigna radiata. Carbohydr Res **265:** 61–77

Hayashi T, Marsden MP, Delmer DP (1987) Pea xyloglucan and cellulose. VI. Xyloglucan-cellulose interactions in vitro and in vivo. Plant Physiol **83:** 384–389

Huster D, Xiao L, Hong M (2001) Solid-state NMR investigation of the dynamics of the soluble and membrane-bound colicin Ia channel-forming domain. Biochemistry **40:** 7662–7674

Ishii T, Matsunaga T (1996) Isolation and characterization of a boron-rhamnogalacturonan-II complex from cell walls of sugar beet pulp. Carbohydr Res **284:** 1–9

Jarvis MC (1992) Self-assembly of plant-cell walls. Plant Cell Environ **15:** 1–5

Kono H, Erata T, Takai M (2003) Determination of the through-bond carbon-carbon and carbon-proton connectivities of the native celluloses in the solid state. Macromolecules **36:** 5131–5138

Li S, Su Y, Luo W, Hong M (2010) Water-protein interactions of an arginine-rich membrane peptide in lipid bilayers investigated by solid-state nuclear magnetic resonance spectroscopy. J Phys Chem B **114:** 4063–4069

Matthews JF, Skopec CE, Mason PE, Zuccato P, Torget RW, Sugiyama J, Himmel ME, Brady JW (2006) Computer simulation studies of microcrystalline cellulose Ibeta. Carbohydr Res **341:** 138–152

McCann MC, Wells B, Roberts K (1990) Direct visualization of cross-links in the primary plant cell wall. J Cell Sci **96:** 323–334

Munowitz MG, Griffin RG, Bodenhausen G, Huang TH (1981) Two-dimensional rotational spin-echo NMR in solids: correlation of chemical shift and dipolar interactions. J Am Chem Soc **103:** 2529–2533

Newman RH, Davies LM, Harris PJ (1996) Solid-state ^{13}C nuclear magnetic resonance characterization of cellulose in the cell walls of *Arabidopsis thaliana* leaves. Plant Physiol **111:** 475–485

Nishiyama Y, Langan P, Chanzy H (2002) Crystal structure and hydrogen-bonding system in cellulose Ibeta from synchrotron x-ray and neutron fiber diffraction. J Am Chem Soc **124:** 9074–9082

Nishiyama Y, Sugiyama J, Chanzy H, Langan P (2003) Crystal structure and hydrogen bonding system in cellulose I(alpha) from synchrotron x-ray and neutron fiber diffraction. J Am Chem Soc **125:** 14300–14306

Oehme DP, Downton MT, Doblin MS, Wagner J, Gidley MJ, Bacic A (2015) Unique aspects of the structure and dynamics of elementary Iβ cellulose microfibrils revealed by computational simulations. Plant Physiol **168:** 3–17

Park YB, Cosgrove DJ (2012a) Changes in cell wall biomechanical properties in the xyloglucan-deficient *xxt1/xxt2* mutant of Arabidopsis. Plant Physiol **158:** 465–475

Park YB, Cosgrove DJ (2012b) A revised architecture of primary cell walls based on biomechanical changes induced by substrate-specific endoglucanases. Plant Physiol **158:** 1933–1943

Peaucelle A, Braybrook S, Höfte H (2012) Cell wall mechanics and growth control in plants: the role of pectins revisited. Front Plant Sci **3:** 121

Popper ZA, Fry SC (2008) Xyloglucan-pectin linkages are formed intraprotoplasmically, contribute to wall-assembly, and remain stable in the cell wall. Planta **227:** 781–794

Rienstra CM, Tucker-Kellogg L, Jaroniec CP, Hohwy M, Reif B, McMahon MT, Tidor B, Lozano-Pérez T, Griffin RG (2002) De novo determination of peptide structure with solid-state magic-angle spinning NMR spectroscopy. Proc Natl Acad Sci USA **99:** 10260–10265

Ryden P, Selvendran RR (1990) Structural features of cell-wall polysaccharides of potato (Solanum tuberosum). Carbohydr Res **195:** 257–272

Somerville C, Bauer S, Brininstool G, Facette M, Hamann T, Milne J, Osborne E, Paredez A, Persson S, Raab T, et al (2004) Toward a systems approach to understanding plant cell walls. Science **306:** 2206–2211

Talbott LD, Ray PM (1992) Molecular size and separability features of pea cell wall polysaccharides: implications for models of primary wall structure. Plant Physiol **98:** 357–368

Tan L, Eberhard S, Pattathil S, Warder C, Glushka J, Yuan C, Hao Z, Zhu X, Avci U, Miller JS, et al (2013) An *Arabidopsis* cell wall proteoglycan consists of pectin and arabinoxylan covalently linked to an arabinogalactan protein. Plant Cell **25:** 270–287

Torchia DA (1978) Measurement of proton-enhanced ^{13}C T_1 values by a method which suppresses artifacts. J Magn Reson **30:** 613–616

van Rossum BJ, de Groot CP, Ladizhansky V, Vega S, de Groot HJ (2000) A method for measuring heteronuclear ^{1}H-^{13}C distances in high speed MAS NMR. J Am Chem Soc **122:** 3465–3472

Wang T, Park YB, Caporini MA, Rosay M, Zhong L, Cosgrove DJ, Hong M (2013) Sensitivity-enhanced solid-state NMR detection of expansin's target in plant cell walls. Proc Natl Acad Sci USA **110:** 16444–16449

Wang T, Salazar A, Zabotina OA, Hong M (2014) Structure and dynamics of *Brachypodium* primary cell wall polysaccharides from two-dimensional ^{13}C solid-state nuclear magnetic resonance spectroscopy. Biochemistry **53:** 2840–2854

Wang T, Williams JK, Schmidt-Rohr K, Hong M (2015) Relaxation-compensated difference spin diffusion NMR for detecting ^{13}C-^{13}C long-range correlations in proteins and polysaccharides. J Biomol NMR **61:** 97–107

Wang T, Zabotina O, Hong M (2012) Pectin-cellulose interactions in the *Arabidopsis* primary cell wall from two-dimensional magic-angle-spinning solid-state nuclear magnetic resonance. Biochemistry **51:** 9846–9856

White PB, Wang T, Park YB, Cosgrove DJ, Hong M (2014) Water-polysaccharide interactions in the primary cell wall of *Arabidopsis thaliana* from polarization transfer solid-state NMR. J Am Chem Soc **136:** 10399–10409

Yao XL, Hong M (2001) Dipolar filtered ^{1}H-^{13}C heteronuclear correlation spectroscopy for resonance assignment of proteins. J Biomol NMR **20:** 263–274

Yao XL, Schmidt-Rohr K, Hong M (2001) Medium- and long-distance ^{1}H-^{13}C heteronuclear correlation NMR in solids. J Magn Reson **149:** 139–143

Zablackis E, Huang J, Müller B, Darvill AG, Albersheim P (1995) Characterization of the cell-wall polysaccharides of *Arabidopsis thaliana* leaves. Plant Physiol **107:** 1129–1138

Zhang T, Mahgsoudy-Louyeh S, Tittmann B, Cosgrove DJ (2014) Visualization of the nanoscale pattern of recently-deposited cellulose microfibrils and matrix materials in never-dried primary walls of the onion epidermis. Cellulose **21:** 853–862

Zhao Z, Crespi VH, Kubicki JD, Cosgrove DJ, Zhong LH (2014) Molecular dynamics simulation study of xyloglucan adsorption on cellulose surfaces: effects of surface hydrophobicity and side-chain variation. Cellulose **21:** 1025–1039

Zykwinska A, Thibault JF, Ralet MC (2007) Organization of pectic arabinan and galactan side chains in association with cellulose microfibrils in primary cell walls and related models envisaged. J Exp Bot **58:** 1795–1802

Zykwinska A, Thibault JF, Ralet MC (2008) Competitive binding of pectin and xyloglucan with primary cell wall cellulose. Carbohydr Polym **74:** 957–961

Zykwinska AW, Ralet MCJ, Garnier CD, Thibault JF (2005) Evidence for in vitro binding of pectin side chains to cellulose. Plant Physiol **139:** 397–407